Contents lists available at ScienceDirect

Journal of Orthopaedic Translation

Original Article

Unveiling the role of CXCL8/CXCR2 in intervertebral disc degeneration: A path to promising therapeutic strategies

Pengfei Xue [a,b,1], Long Lv [c,1], Lei Liu [b], Yuzhu Xu [a,b], Chonggang Zhou [d,**], Yuntao Wang [b,*]

[a] Medical School of Southeast University, Nanjing, Jiangsu, 210009, China
[b] Department of Spine Center, Zhongda Hospital, Southeast University, Nanjing, Jiangsu, 210009, China
[c] Central Laboratory, Gaochun Hospital Affiliated to Jiangsu University, Nanjing, Jiangsu, 211300, China
[d] Department of Orthopedics, Jiujiang Traditional Chinese Medicine Hospital, Jiujiang, Jiangxi, 332000, China

ABSTRACT

Background: Intervertebral disc degeneration(IVDD) is the primary etiology of low back pain and radicular pain. Recent studies have found that chemokines play a role in IVDD, but the underlying mechanism is largely unclear.
Methods: Bioinformatics analysis was employed to screen CXCL8 as the target gene. The expression levels of CXCL8 and CXCR2 were quantified using RT-qPCR, western blot(WB), immunohistochemistry(IHC), and enzyme-linked immuno-sorbent assay(ELISA). In the IVDD mouse model, X-ray images, Safranin O-fast green staining(SO-FG), IHC, and WB were conducted to assess the therapeutic effects of CXCL8 on IVDD. Reactive oxygen species (ROS) production, apoptosis of nucleus pulposus cells (NPCs), and the involvement of the NF-κB pathway were evaluated through WB, flow cytometry, immunofluorescence(IF), and Tunnel assay.
Results: In our study, we observed that CXCL8 emerged as one of the chemokines that were up-regulated in IVDD. The mitigation of extracellular matrix degradation (ECM) and the severity of IVDD were significantly achieved by neutralizing CXCL8 or its receptor CXCR2(SB225002, CXCR2 antagonist). The release of CXCL8 from infiltrated macrophages within intervertebral discs (IVDs) was predominantly observed upon stimulation. CXCL8 exerted its effects on NPCs by inducing apoptosis and ECM degradation through the activation of CXCR2. Specifically, the formation of the CXCL8/CXCR2 complex triggered the NF-κB signaling pathway, resulting in an abnormal increase in intracellular ROS levels and ultimately contributing to the development of IVDD.
Conclusion: Our findings suggest that macrophage-derived CXCL8 and subsequent CXCR2 signaling play crucial roles in mediating inflammation, oxidative stress, and apoptosis in IVDD. Targeting the CXCL8/CXCR2 axis may offer promising therapeutic strategies to ameliorate IVDD.
The translational potential of this article: This study indicates that CXCL8 can effectively exacerbate the excessive apoptosis and oxidative stress of NPCs through activating the NF-κB pathway. This study may provide new potential targets for preventing and reversing IVDD.

1. Introduction

Intervertebral disc degeneration (IVDD) is a prominent etiology of low back pain, recognized as the leading cause of years lived with disability worldwide [1]. The degenerative process of the nucleus pulposus (NP), the central gelatinous component of the IVDs, plays a pivotal role in the pathogenesis of IVDD [2,3]. Presently, the management strategies and treatments for IVDD predominantly concentrate on pain alleviation, lacking the ability to achieve substantial and enduring therapeutic outcomes [4,5]. Consequently, the persistent menace presented by IVDD to human well-being has spurred the pursuit of a heightened comprehension of IVD physiology and pathology.

The activation of the innate immune system is provoked by a localized inflammatory environment and the rupture of the annulus fibrosus (AF), which is caused by various factors [6,7]. This activation leads to a persistent inflammatory response within the IVDs. Infiltration of the macrophages releases a variety of inflammatory mediators, which posseses potent chemotaxis angiogenesis and pain mediator secretion
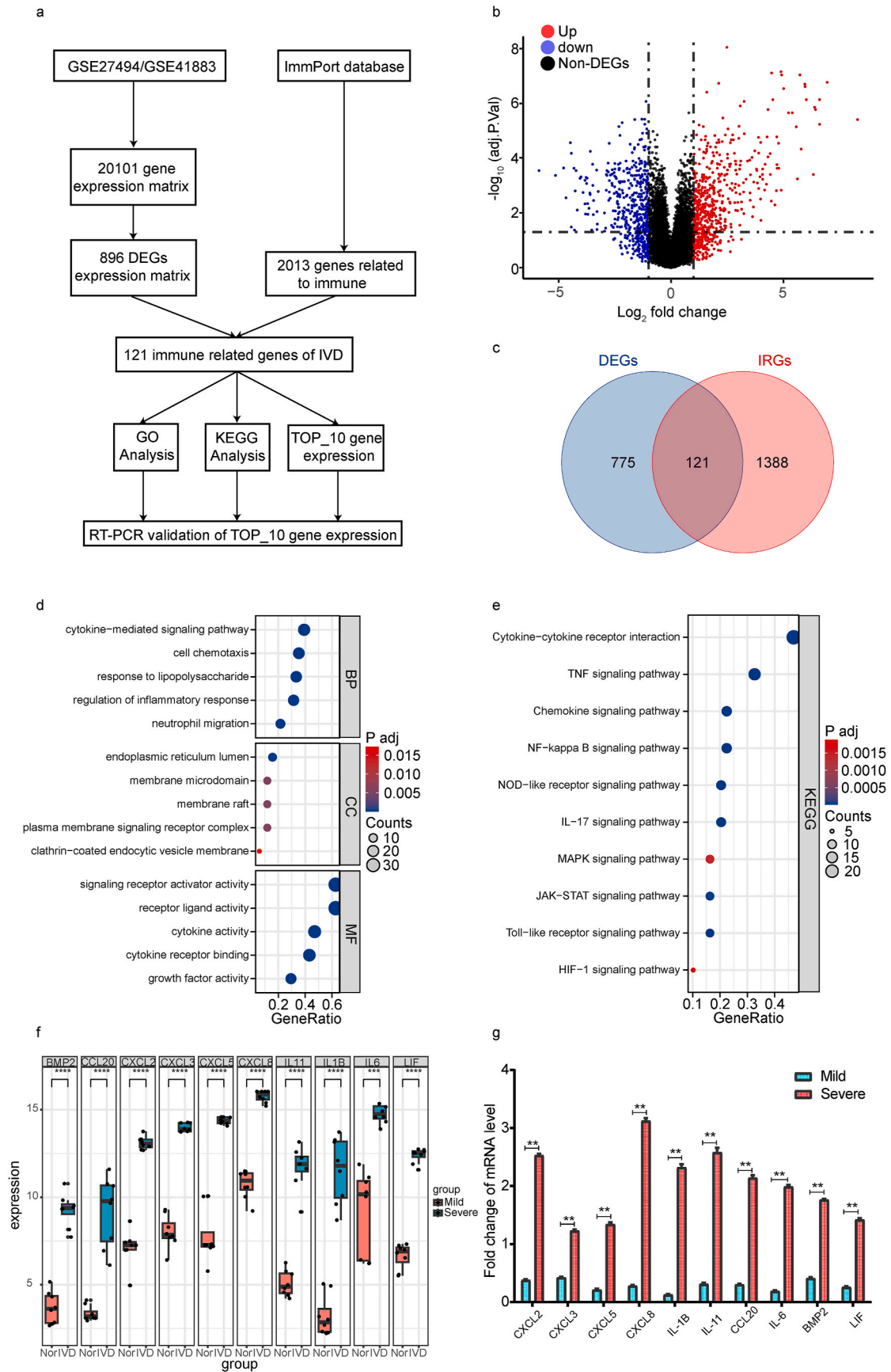
(caption on next page)

Fig. 1. Identification of CXCL8 associated with intervertebral disc degeneration in GSE27494/GSE41883.
(a) Flowchart of bioinformatics analysis in GSE27494/GSE41883. (b) Volcano plot of differentially expressed genes (DEGs). Red represented up-regulated expression, green represented down-regulated expression, and black represented no difference. (c) Venn diagram between DEGs and immune-related DEGs (IRGs). (d–e) Significantly enriched GO terms and KEGG pathways of the IRGs. (f) Top_10 differentially expressed immune related DEGs in IVDD. The green box plots represented the expression in severe IVDD patients, whereas the red box plots represented the expression in mild IVDD patients. (g) qRT-PCR validation of candidate top_10 gene expression in degenerative IVDs (N = 3 Severe degenerative group(SD), N = 3 mild degenerative group(MD)). Data are represented as fold changes ±s.e.m and were analysed using two-tailed unpaired t-test. **$p < 0.01$ SD group vs MD group. (For interpretation of the references to color in this figure legend, the reader is referred to the Web version of this article.)

capabilities, resulting in neovascularization around the damaged IVD [8,9]. Under the influence of pain mediators, neovascularization stimulates the growth of local nerves, which is considered one of the potential causes of discogenic back pain [10]. However, it still remains elusive how inflammatory mediators are generated in the inflamed tissues in the context of IVDD.

In the present study, we conducted an analysis of the combined GSE27494/GSE41883 datasets to screen and validate CXCL8 as a prominent inflammatory mediator. CXCL8 is primarily secreted by macrophages, T-lymphocytes, neutrophils, and other cells in response to an antigen [11]. It interacts with chemokine receptors CXCR1 and CXCR2 [12]. Within IVDs, elevated levels of CXCL8 are observed due to oxidative/nitrosative stress and mechanical stress-induced damage [13]. The increased CXCL8 levels contribute to hyperalgesia by promoting the local production of sympathetic amines, thereby enhancing the sensitivity of nociceptors [14]. We aimed to explore the potential mechanism that CXCL8/CXCR2 mediates IVDD progression through promoting ROS production and apoptosis of NPCs.

2. Materials and methods

2.1. Ethics declarations and patient specimens obtain

Human disc tissue collection and experiments were approved by the Institutional Review Board (IRB) of the Zhongda Hospital Affiliated with the Southeast University (approval: 2023ZDSYLL189-P01) and registered in clinical trial (approval: NCT05976516). Procedures followed were in accordance with the ethical standards of the responsible committee on human experimentation and with the Helsinki Declaration of 1975, as revised in 2000. All tissue samples obtained from patients were collected after informed consent. The patients and their families were duly informed about the intention to publish data derived from their cases and provided their consent accordingly.

Degenerative NP tissues were procured from patients who underwent surgery for IVDD. The specimens were promptly divided into sections to facilitate their utilization in diverse experiments. The patient's demographic characteristics, such as gender, age, body mass index (BMI), Visual Analogue Scale (VAS), and Oswestry Disability Index (ODI), were documented. Additionally, the intervertebral disk height at the degenerated segment on CT/MRI imaging, as well as the grade of degeneration and cross-sectional area (CSA) of fatty infiltration in the spinal paravertebral muscles including Lumbar Multifidus muscle (LMM); Psoas major muscle (PM), were recorded. For further details, please consult supplementary materials (Table S1) for supplementary general information.

2.2. Animals and IVDD models

All experimental protocols were reviewed and approved by the Animal Care Committee of the Southeast University (approval:20220224016) in accordance with the Institutional Animal Care and Use Committee guidelines (Southeast University, nanjing, China). A total of 64 Male Sprague Dawley rats (3 months old and weighing 450 g) were purchased from the Animal Laboratory Center of Southeast University, Nanjing, China. The rats were raised under pathogen free conditions and maintained in a 12-h light/dark cycle. Rats were randomly divided into the following groups: Normal group (no

needle puncture; no injection); IVDD group (needle puncture; no injection); IVDD + CXCL8 Ab group (needle puncture; CXCL8 Ab injection); IVDD + SB225002 group (needle puncture; SB225002 injection); IVDD + r-CXCL8 group (needle puncture; r-CXCL8 injection); IVDD + r-CXCL8+SB225002 group (needle puncture; r-CXCL8+SB225002 injection). As previously described, following anesthesia with isoflurane, a 26G needle was inserted through AF into the tail skin, targeting CO6/7 or CO7/8 or CO8/9 using a M60 microscope (Leica Microsystems, IL, USA). After surgery, rats were closely observed postoperatively to detect any potential complications [15]. Mouse IVDD model was constructed in supplementary materials.

2.3. Reverse transcription and quantitative realtime PCR

Total RNA was extracted from human disc tissues and cultured cells using TRIzol reagent, followed by reverse transcription in accordance with the instructions provided by the manufacturer(TaKaRa, Japan). Polymerase Chain Reaction (PCR) was conducted in a reaction volume of 20 μL utilizing PCR mix (TaKaRa, Japan), and PCR amplification was executed employing a PCR cycler (ABI, USA). The human primer sequences were listed in the supplementary materials (Table S2).

2.4. Enzyme-linked immuno-sorbent assay (ELISA)

The assays were performed in accordance with the guidelines provided by the manufacturer, employing a sample volume of 100 μL. NP samples and cells were collected post-treatment, weighed, and promptly frozen in liquid nitrogen. Tissues were homogenized at a temperature of 4 °C, followed by centrifugation of the resulting supernatants at 12,000 g for a duration of 15 min at 4 °C. Duplicate measurements of the supernatants were subjected to ELISA analysis for CXCL8, utilizing a commercially available kit (R&D Systems, Minneapolis, MN, USA), as per the manufacturer's instructions.

2.5. Western Blotting (WB)

WB was performed according to the previously described method [16]. In brief, the total protein from NP tissues and cells was extracted using a cell lysis buffer. Subsequently, the protein samples were loaded onto SDS-PAGE gels (10–12 %) and transferred onto PVDF membranes. The membranes were then blocked with 5 % skimmed milk at room temperature for 2 h and incubated with specific first primary antibodies overnight at 4 °C. The primary antibodies used for incubation were as follows: Human anti-CXCL8 antibody (1:500, R&D Systems), Human and mouse anti-CXCR2 antibody (1:1000, R&D Systems), Rabbit anti-GAPDH antibody (1:5000, PEPROTECH), Rabbit anti-MMP13 antibody (1:1000, Abcam), Rabbit anti-COL2A1 antibody (1:1000, Abcam), Rabbit anti-P65 antibody (1:2000, CST), Rabbit anti-p-P65 antibody (1:2000, CST), Rabbit anti-IKBa antibody (1:2000, CST), Rabbit anti-p-IKBa antibody (1:2000, CST). The respective secondary antibody were incubated for 2 h. After washing in TBST, the protein was visualized using ultra-sensitive ECL kit (Bio-Rad).

2.6. Histological analysis of IVD

The NP tissues and IVDs were surgically excised and promptly fixed in a 4 % PFA solution for 48 h. Subsequently, decalcification was carried
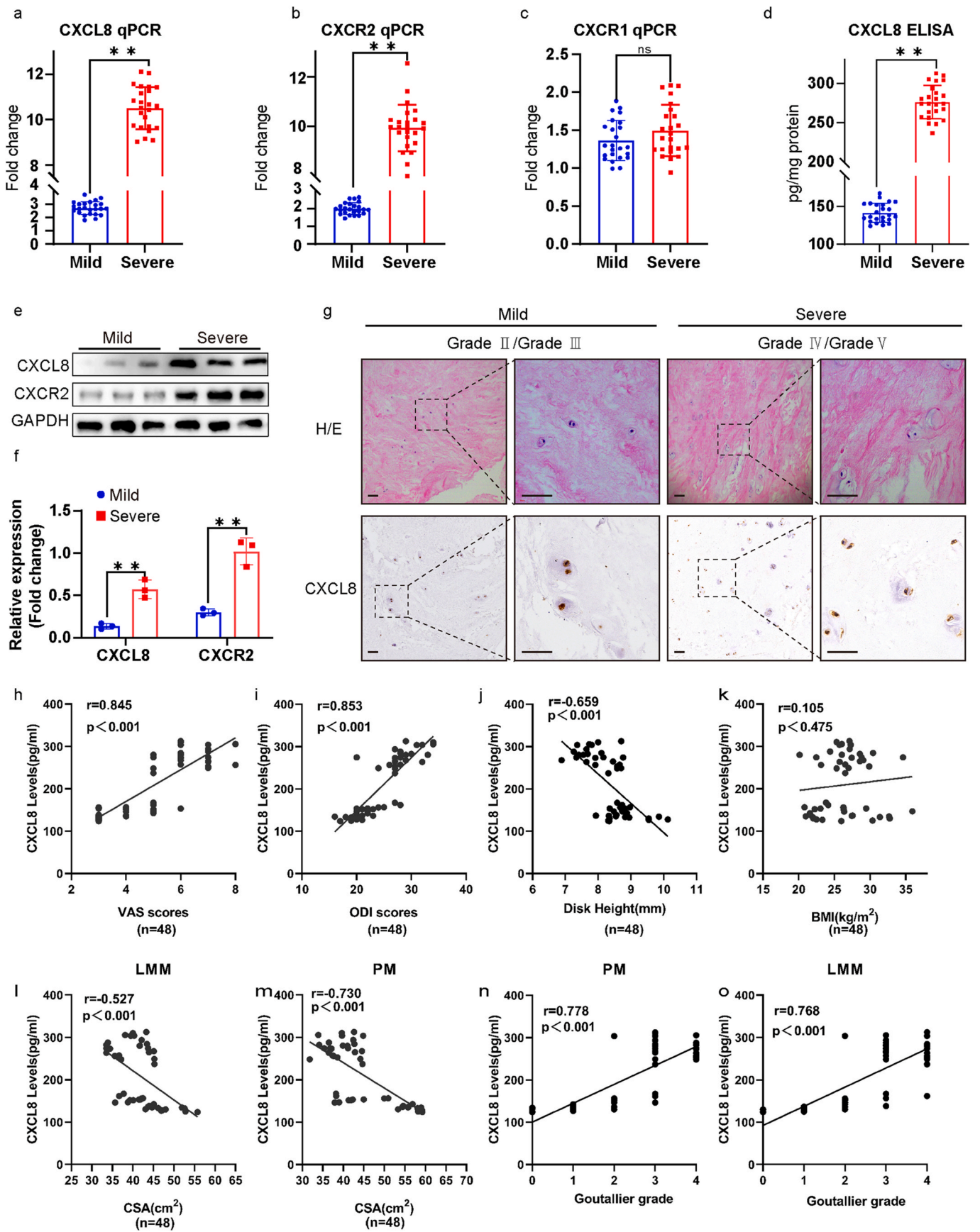
(caption on next page)

Fig. 2. The expressions of CXCL8 and CXCR2 were up-regulated in nucleus pulposus(NP) tissues of IVDD.
(a–c) qRT-PCR analysis of CXCL8, CXCR2 and CXCR1 mRNA expression levels in NP tissues of Mild group and Severe Group (N = 24 for each group). (d) ELISA analysis of CXCL8 concentrations of Mild group and Severe Group (N = 24 for each group). (e–f) Western blot detection (e) and grey value analysis (f) of CXCL8 and CXCR2 level in Mild group and Severe Group (N = 3 biological samples for each group). (g) Representative images of hematoxylin-eosin staining (H&E) and immunohistochemical staining (IHC) (N = 3 slides for each group; scale bar: 4x left; 40x right). (h–k) Pearson's correlation of CXCL8 concentrations with VAS scores, ODI index, disk height(mm) and BMI(kg/m^2) of enrolled individuals (N = 48 for each group). (l–o) Pearson's correlation of CXCL8 concentrations with LMM and PM degeneration, CSA and Goutallier grade (N = 48 for each group). Data are represented as mean ± s.e.m and were analysed using two-tailed unpaired t-test(a,b,c,d,f), two-tailed Pearson's correlation analysis (h–o). Significant differences between the groups are indicated as **$p < 0.01$, ns: no significance. Notes: VAS: Visual Analogue Scale, ODI: Oswestry Disability Index, BMI: body mass index, LMM: lumbar multifidus muscle, PM: psoas major muscle,CSA: cross-sectional area.

out using a 10 % EDTA solution (BOSTER, China). Once decalcification was completed, the specimens were dehydrated, embedded in paraffin wax, and sectioned into 8 μm slices. A subset of these tissue sections was subjected to hematoxylin and eosin (H/E) staining, while another subset was utilized for Safranin O–fast green (SO-FG) staining. The remaining sections were designated for immunohistochemical (IHC) analysis. Following the manufacturer's instructions, the sections were incubated with the appropriate antibodies: Human anti-CXCL8 antibody (1:200, R&D Systems); Mouse anti-CXCR2 antibody (1:300, R&D Systems); Rabbit anti-MMP13 antibody (1:200,Abcam); Rabbit anti-COL2A1 antibody (1:200,Abcam), then incubated with secondary antibody. Tissue sections were observed with an upright microscope (Nikon, Japan). To assess the degeneration of IVDs, six blinded observers evaluated mid-coronal sections from three caudal disc levels using a modified histological grading scale [17].

2.7. Primary nucleus pulposus cells (NPCs) culture

Nucleus pulposus cells (NPCs) were obtained from the NP tissue of 4-week-old Sprague–Dawley rats (n = 4). The NP tissue was carefully excised from the IVDs, then minced and enzymatically digested with 0.1 % collagenase (Gibco, Shanghai, China) at 37 °C for 20 min. The digestion was halted by adding Dulbecco's modified Eagle's medium: F-12 (Gibco), followed by centrifugation at 1000g for 5 min. Primary culture was established using DMEM/F12 in a humidified incubator at 37 °C with 5 % CO_2. The medium was refreshed every other day, and passaging was performed once the cell density reached 80 %. The third generation of cells was used in subsequent experiments.

2.8. Immunofluorescence (IF)

For immunofluorescence (IF), the paraffine embedded samples were dewaxed and rehydrated. After sealed for 2 h blocking buffer consisted of 5 % bovine serum albumin (BSA) diluted by phosphate buffer solution (PBS) and incubated with primary antibodies: Mouse anti-CXCR2 antibody (1:300, R&D Systems), Rabbit anti-F4/80 antibody (1:300, Abcam) with 1 × PBS at 4 °C overnight. Then the sections were rinsed by PBS and incubated with corresponding secondary antibodies. Finally, images were collected under fluorescence microscope (Leica, DM 5000B; Germany).

Cells were fixed with 4 % paraformaldehyde for 15 min followed by PBS, and 0.2 % Triton X-100 (W/V) in PBS was added for 15 min. Cells were blocked with 5 % BSA for 30 min. Primary antibodies against Mouse anti-CXCR2 antibody (1:300, R&D Systems) and Rabbit anti-cleaved-caspase3 antibody (1:300, Abcam) or Rabbit anti-P65 antibody (1:500, CST) were added followed by incubation at 4 °C for 12 h. Remaining steps were as previously described.

2.9. TUNEL assay

TUNEL staining was used to analyse cell apoptosis. For the preparation of paraffin sections, the sections were first deparaffinized and rehydrated before being incubated with protein Kinase (20 μg/mL) for 15 min at 37 °C. Subsequently, the sections were washed with PBS and stained using TUNEL staining. Finally, the assessment of apoptotic cells was conducted using a confocal microscope (A1R; Nikon).

2.10. Flow cytometry

The apoptosis rate of NPCs was assessed using the Annexin V-FITC/PI Apoptosis Detection Kit (Beyotime; C1062). Following trypsinization, NPCs were resuspended in 500 μL of binding buffer, and subsequently, 5 μL of Annexin V-FITC and PI were added. After a 10-min incubation in the dark at room temperature, the apoptosis rate was analyzed using the FACSCanto Analyzer (BD Biosciences).

2.11. Reactive oxygen species (ROS) levels

ROS detection was performed using the fluorescent probe Dichlorodihydrofluorescein diacetate (DCFH-DA). DCFH-DA was diluted 1:1000 in serum-free medium to a final concentration of 10 μmol/L. The cell culture medium was removed and an appropriate volume of diluted DCFH-DA was added. NPCs of each group were incubated in a 37 °C incubator for 20 min. NPCs were washed 3 times with serum-free cell culture medium to sufficiently remove DCFH-DA that did not enter the cells. Intracellular ROS content was measured by flow cytometry using DCFH-DA.

2.12. Statistical analysis

Statistical analysis was performed using GraphPad Prism 9 (La Jolla, CA, USA). The results were presented as the mean ± standard error of the mean(s.e.m). Statistical significance between two groups with parametric data was evaluated using two-tailed, unpaired Student's T-tests when homogeneity of variances was assumed ($p > 0.05$) based on the F-test, and with Welch's t-test when homogeneity of variances was not assumed ($p < 0.05$) based on the F-test. Statistical analysis was conducted to compare multiple groups with parametric data using one-way analysis of variance (ANOVA) followed by Tukey's multiple comparisons post-hoc tests. Kruskal–Wallis H test with Dunn's post-test was used to analyze histological score, which did not conform to the normal distribution. Correlation analysis was conducted using Pearson's correlation coefficient. A P-value less than 0.05 (P < 0.05) was considered statistically significant.

3. Results

3.1. CXCL8 is highly expressed in NP tissues from IVDD patients

Fig. 1a showed the bioinformatics analysis flowchart of GSE27494 and GSE41883. Based on the analysis, 20101 genes were identified, including 896 differentially expression genes (DEGs). A total of 2013 immune related genes (IRGs) were selected from the ImmPort database, of which 121 could be matched in the expression profile of DEGs. The volcano plot of GSE27494/GSE41883 and the Venn diagram were shown in Fig. 1b and .c. The IRGs were analyzed by gene ontology (GO) and Kyoto Encyclopedia of Genes and Genomes (KEGG) to determine their roles in IVDD. GO analysis showed that they were mainly enriched in cytokine-mediated signaling pathway, endoplasmic reticulum lumen, signaling receptor activator activity and so on (Fig. 1d). In KEGG pathway annotations, the targeted genes were highly enrolled in a number of pathways, such as Cytokine–cytokine receptor interaction, TNF signaling pathway, Chemokine signaling pathway and NF-kappa B
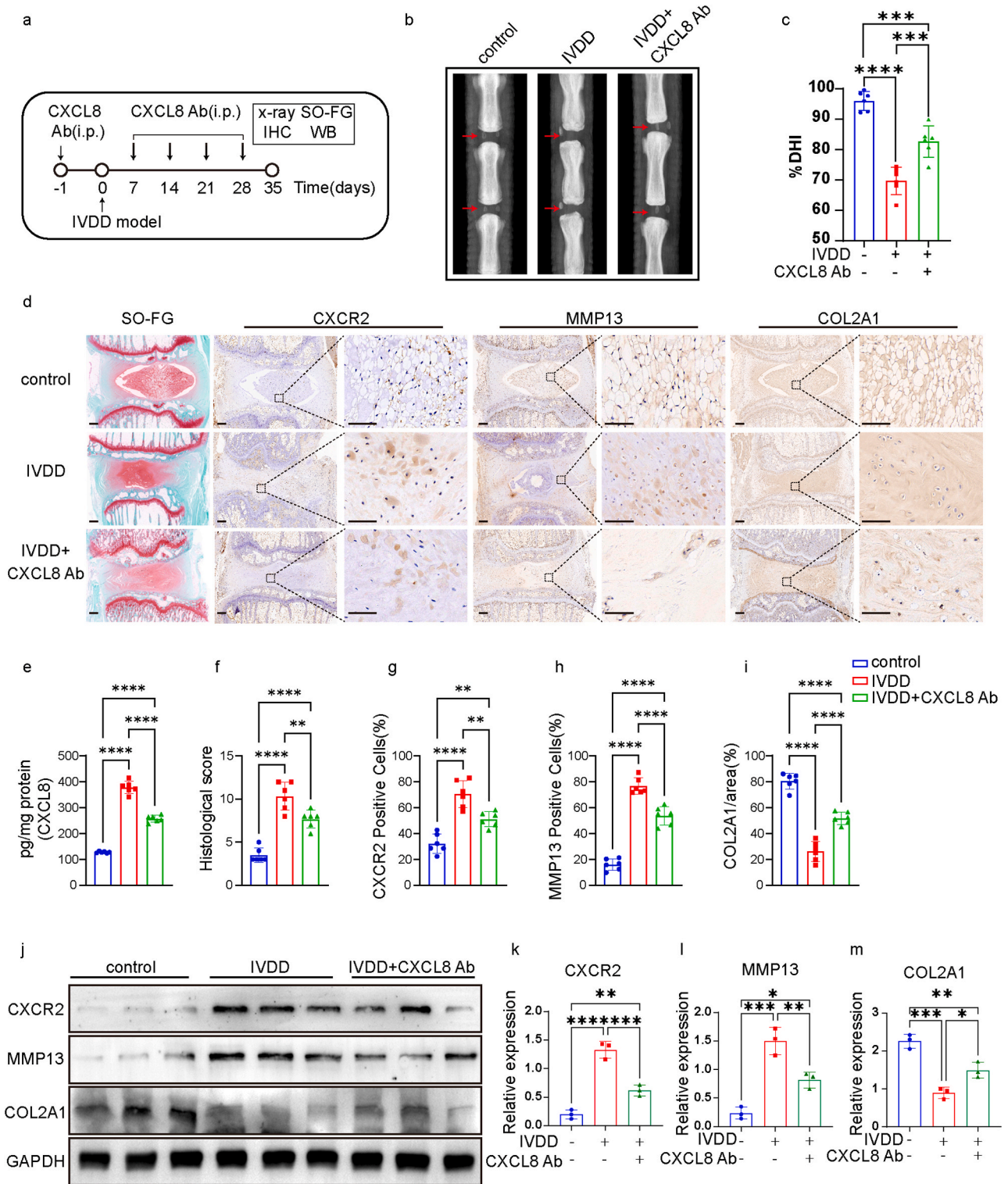
Fig. 3. CXCL8 neutralizing antibody alleviated intervertebral disc degeneration

(a) Schematic diagram illustrating the design of the CXCL8 Ab experiments. (b–c) Representative X-ray images (b, red arrow represents the modeled segment) and % DHI (c) in control group, IVDD group and CXCL8 Ab group (N = 6 for each group). (d) Representative images of Safranin O-fast green staining (SO-FG) and IHC. Regions within black boxes (left) were amplified at right. Scale bar (left) = 400 μm. Scale bar(right) = 50 μm. (e) CXCL8 content in different groups of NP (N = 6 for each group). (f–i) The histological score of the sections, the number of CXCR2/MMP13 positive cells and COL2A1 positive area in each group (N = 6 for each group). (j–m) Western blot detection (j) and grey value analysis (k–m) of CXCR2/MMP13/COL2A1 level in control group, IVDD group and CXCL8 Ab group (N = 3 biological samples for each group). Data are represented mean ± s.e.m and were analysed using one-way ANOVA followed by Tukey's multiple-comparison test(c, e, g-i, k-m), histological score was analysed by Kruskal–Wallis with Dunn's post-test. $*p < 0.05$, $**p < 0.01$, $***p < 0.0001$, $****p < 0.00001$ were considered significant differences. (For interpretation of the references to color in this figure legend, the reader is referred to the Web version of this article.)
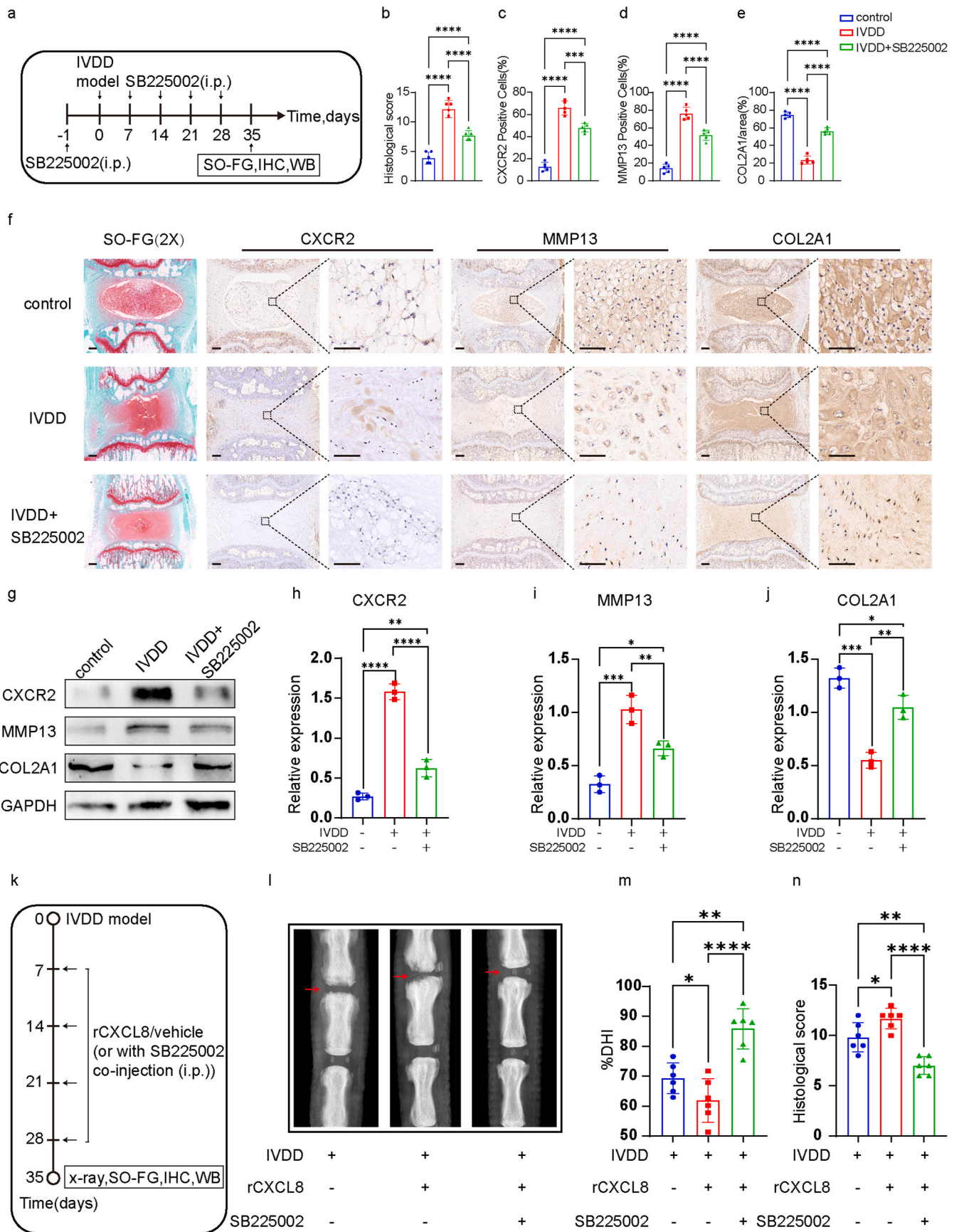
(caption on next page)

Fig. 4. CXCL8/CXCR2 signaling is involved in mediating extracellular matrix degradation of the IVDD model

(a) Schematic picture depicting the time points of SB225002 (selective CXCR2 antagonist) administration and SO-FG/IHC/WB tests. (b–f) Representative images of SO-FG and IHC (f). Regions within black boxes on the left were magnified on the right. Scale bar (left) = 400 μm. Scale bar (right) = 50 μm. Histological scores(b) for the sections, the number of CXCR2 (c)/MMP13 (d) positive cells and COL2A1 positive area (e) in control group, IVDD group and SB225002 group (N = 5 for each group). (g–j) Western blot detection (g) and grey value analysis (h–j) of CXCR2/MMP13/COL2A1 level (N = 3 biological samples for each group). (k) Schematic diagram illustrating the design of the loss-gain function experiments. (l–n) Representative X-ray images (l), %DHI (m) and histological score (n) of the sections in IVDD group, IVDD + r-CXCL8 group and IVDD + r-CXCL8+SB225002 group (N = 6 for each group). Data are represented mean ± s.e.m and were analysed using one-way ANOVA followed by Tukey's multiple-comparison test (c-e, h-j, m), histological score was analysed by Kruskal–Wallis with Dunn's post-test (b and n). *p < 0.05, **p < 0.01, ***p < 0.0001, ****p < 0.00001 were considered significant difference.

signaling pathway (Fig. 1e). Based on the LogFC values of each gene in the datasets, we selected the 10 candidate genes with highest expression (Fig. 1f). Among these genes, IL-6, IL-1β and CXCL3 were previously widely believed to be closely related to inflammation and significantly increased in the IVDD group [14,18,19]. In an attempt to explore the potential role of cytokines in IVDD pathogenesis, we collected a total of 48 NP samples from IVDD patients and validated the expression of the candidate top_10 genes.

In this study, patients with IVDD were enrolled between May 2022 and December 2022. The human NP degeneration grade and the general morphology was determined by MRI (Fig. S1). Based on the pfirrmann classification [20], we divided the degenerated nucleus pulposus into two groups: mild IVDD group and severe IVDD group. As shown in Table S1, there were no significant differences in age (Y), gender (F/M), and BMI (kg/m^2) between the two groups (Table S1). We validated the expression of the 10 candidate genes described previously, CXCL8 showed the highest expression compared to the mild group (Fig. 1g). The results of the correlation analysis revealed a positive correlation between CXCL8 and IL-1β, IL-6, MMP3, and RUNX2, while a negative correlation was observed between CXCL8 with COMP and ACAN (Fig. S2). These findings suggested that CXCL8 potentially play a role in the regulation of extracellular matrix equilibrium within the NP. CXCL8 was previously reported to be highly expressed in degenerative IVDs and often associated with higher VAS scores [21,22], but the mechanism by which it regulated IVDD remained unclear. Considering this, we investigated the possible role of CXCL8 in IVDD.

As shown in Fig. 2a, CXCL8 was significantly increased in NP tissue of the severe IVDD group by qRT-PCR. CXCR2 not CXCR1, the specific receptor for CXCL8, was significantly upregulated as well (Fig. 2b–c). Based on ELISA results, severe IVDD group showed increased CXCL8 protein levels (Fig. 2d). WB further indicated CXCL8 protein expression was significantly increased in NP tissues of severe IVDD group (Fig. 2e–f). NP tissue degeneration grade was further confirmed by H/E staining and IHC. In severe IVDD group, CXCL8 was highly expressed (Fig. 2g). To further evaluate the correlation between CXCL8 and clinical symptoms and paraspinal muscle degeneration, we conducted statistical analysis on the preoperative VAS score and ODI index of two groups. VAS score and ODI index was higher in severe IVDD group compared with mild IVDD group (Table S1). CXCL8 concentrations positively correlated to VAS score and ODI index (Fig. 2h–i). In addition, we also compared CXCL8 concentrations with intervertebral disk height (%DHI) and BMI, we found a significant negative correlation between %DHI and CXCL8, indicating that higher levels of CXCL8 tend to cause intervertebral space collapse (Fig. 2j). BMI has no significant correlation with CXCL8 (Fig. 2k). Previous studies have described a close correlation between fat infiltration in multifidus muscle and local inflammatory factors [23]. The degeneration grade of lumbar multifidus muscle (LMM) and psoas major muscle (PM) were evaluated by Goutallier grade [24], and their cross-sectional area (CSA) was calculated. As Fig. 2l-m shown, CXCL8 concentrations were significantly negative relative to LMM and PM. We further compared CXCL8 concentrations among different Goutallier grade. In both LMM and PM degeneration, CXCL8 concentrations were positively correlated with fat tissue infiltration as measured by Goutallier grade (Fig. 2n-o). These results all suggested that CXCL8 may be involved in the progression of IVDD.

3.2. CXCL8/CXCR2 signaling is involved in progression of IVDD

We conducted a study to investigate the potential involvement of CXCL8 in IVDD model. Rats were administered with a CXCL8 neutralizing antibody (5 μg/rat, i.p.) or an isotype control IgG (goat IgG, 5 μg/rat, i.p.) one day prior to model establishment and at 7, 14, 21, and 28 days thereafter (Fig. 3a). X-ray imaging showed that treatment with a CXCL8 neutralizing antibody delayed the disc height loss induced by puncture surgery. It significantly alleviated IVDD including %DHI at 35 day (Fig. 3b–c). SO-FG staining revealed a significant disruption in the texture of the tissue in the IVDD group, characterized by the presence of hypertrophic and vacuole-like cells, as well as a multinuclear giant cell at the distal end of the sample. SO-FG staining demonstrated reduced levels of proteoglycans (PGs) and elevated levels of fibrosis in the nucleus pulposus (NP) tissues of the IVDD group. The administration of a CXCL8 neutralizing treatment not only caused the decrease of CXCL8 concentrations (Fig. 3e) but also resulted in the mitigation of degenerative manifestations within the IVDs, including a decrease substitution of NPCs with fibrochondrocytes, and the collapse of cartilage endplates (Fig 3d and f-i). These findings provide confirmation that severely degenerated NP tissue is strongly associated with a high degeneration grade. Moreover, the application of IHC and WB demonstrated that the administration of a CXCL8 neutralizing antibody resulted in a significant reduction in CXCR2 and MMP13 expression, while concurrently increasing the expression of COL2A1 (Fig. 3j-m). These outcomes provide substantial evidence supporting the notion that CXCL8 accumulates within the NP tissues as IVDD progressing.

We further examined the effects of SB225002 (selective CXCR2 antagonist) on IVDD. Rats were administered with SB225002 (2 mg/kg, i.p.) or DMSO one day prior to model establishment and at 7, 14, 21, and 28 days thereafter (Fig. 4a). Similarly, SB225002 treated rats exhibited reduced histological scores compared with IVDD group (Fig. 4b). SO-FG staining showed typical disc degeneration phenotype with the loss of NP cells and matrix in IVDD group. The application of SB225002 can partially reverse the process of IVDD. As expected, IHC staining revealed that the expression of CXCR2 and MMP13 was significantly decreased in SB225002 administration group compared with IVDD group (Fig. 4c–f). WB showed that in contrast to IVDD group, the expression of CXCR2 and MMP13 in degenerated IVDs was significantly lower, while the expression of COL2A1 was much higher (Fig. 4g–j). In the subsequent rescue experiment, we injected recombinant CXCL8 (rCXCL8) and SB225002 together to observe the X-ray, SO-FG, IHC and WB of the IVDs (Fig. 4k). X-ray showed the administration of rCXCL8 leads to additional degradation of intervertebral space height and substantial disc destruction, while the application of SB225002 can effectively counteract this alteration (Fig. 4l-m). Similarly, SO-FG staining showed SB225002 can partially reverse the process of IVDD induced by rCXCL8, IHC staining revealed that the expression of CXCR2 and MMP13 was significantly decreased in SB225002 administration group compared with IVDD + rCXCL8 group, the expression of COL2A1 exhibited an inverse pattern (Fig. S3a and c-e). WB showed that in contrast to IVDD + rCXCL8 group, the expression of CXCR2 and MMP13 in degenerated IVDs was significantly lower, while the expression of COL2A1 was much higher (Fig. S3b and f-h). SB225002 significantly reduced the histological score of IVDD caused by rCXCL8 injection (Fig. 4n). Therefore, these data suggest that CXCL8 acts on CXCR2 to exacerbate inflammation and extracellular
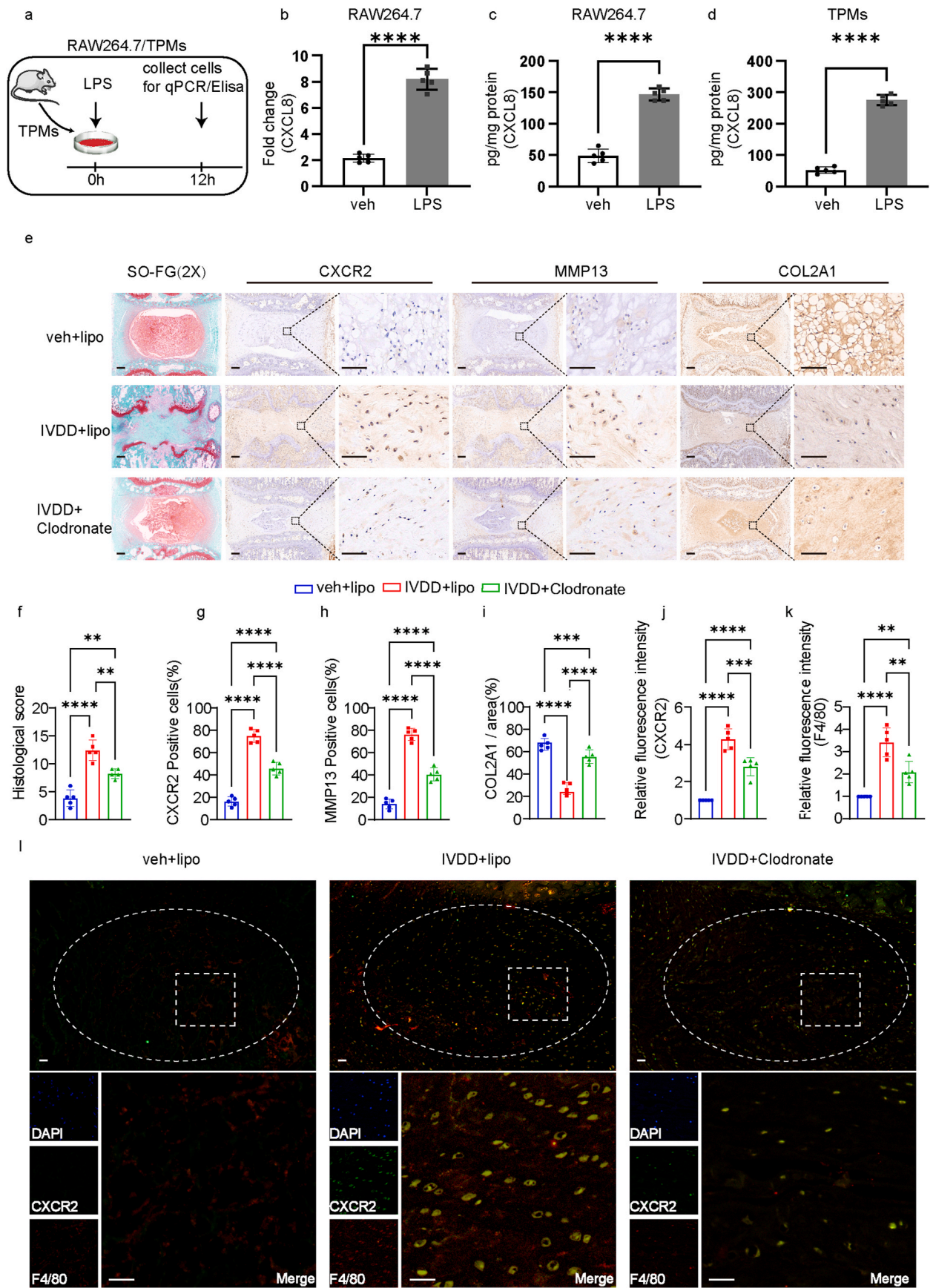
(caption on next page)

Fig. 5. Macrophage is among one of the cellular mchanisms for CXCL8 production in IVDD

(a) Schematic protocol illustrating time points for RAW264.7 and Thioglycollate-elicited macrophages (TPMs) cell harvest. (b–d) Expression of CXCL8 mRNA in RAW264.7 cells after LPS (1 μg/ml) incubation by qRT-PCR (b). CXCL8 concentration in RAW264.7 cells and TPMs after LPS incubation by ELISA (N = 5 for each group). (e–i) Representative images of SO-FG and IHC (e). Regions within black boxes on the left were magnified on the right. Scale bar (left) = 400 μm. Scale bar (right) = 50 μm. Histological scores (f) for the sections, the number of CXCR2 (g)/MMP13 (h) positive cells and COL2A1 positive area (i) in control group, IVDD group and IVDD + Clodronate group (N = 5 IVD slices for each group). (j–l) Immunofluorescence (IF) assays for CXCR2 (green), F4/80 (red), and Nucleus (blue) in IVD. Scale bar = 400 μm (above), Scale bar = 100 μm (below). Co-localization analysis by evaluating relative fluorescence intensity (j and k). Data are represented mean ± s.e.m and were analysed using two-tailed unpaired t-test(b,c,d), one-way ANOVA followed by Tukey's multiple-comparison test(g-k), histological score was analysed by Kruskal–Wallis with Dunn's post-test (f). **p < 0.01, ***p < 0.0001, ****p < 0.00001 were considered significant difference. (For interpretation of the references to color in this figure legend, the reader is referred to the Web version of this article.)

matrix degradation in rats IVDD model.

3.3. Macrophage is among one of the cellular mchanisms for CXCL8 production in IVDD

Inflammatory state, macrophages accumulate in the IVDs, secrete large amounts of chemokines, cause vascularization and produce pain mediators, resulting in low back pain [2,9]. Macrophages within the IVDs are the main source of CXCL8 [22]. In vitro, we initially examined the impact of LPS (1 μg/ml) on the RAW264.7 macrophage cell line. As a means of comparison, exposure to LPS resulted in a noticeable increase in CXCL8 expression as observed through qRT-PCR and ELISA, in contrast to the vehicle (PBS) group (Fig. 5b–c). Subsequently, we proceeded to investigate the impact of LPS on mouse macrophages. We obtained Thioglycollate-elicited macrophages (TPMs) from mice, which were verified to possess a macrophage purity of over 90 % examined by IF (Fig. S4). Following incubation with LPS, a notable augmentation in CXCL8 protein expression was observed in TPMs (Fig. 5d). Additionally, we examined the effect of in vivo macrophages depletion using clodronate-containing liposomes on CXCL8 release in IVDD (Fig. S5a). Clodronate administration (1mg/100 μl,i.p.) significantly decreased the presence of macrophages, as indicated by F4/80 staining, in the spleen of mice compared to the control group receiving liposome treatment (Figs. S5b–d). This finding highlights the efficacy of clodronate in depleting macrophages. The NP tissues were then collected and subjected to protein detection. Clodronate induced macrophage depletion significantly reduced the upregulation of CXCR2 and MMP13 protein expression from IVDD group, significantly elevated COL2A1 expression (Figs. S5e–h). The degree of disc degeneration in the IVDD group was further alleviated by clodronate-induced macrophage depletion, as evidenced by SO-FG staining and IHC(Fig. 5e–i). Furthermore, mice treated with puncture needle exhibited noticeable macrophage accumulation in the tissue surrounding the NP, which was significantly reduced following clodronate treatment, dual immunofluorescence of CXCL8 or CXCR2 with F4/80 confirmed this result (Fig. 5j-l and Figs. S5i–k). Based on the aforementioned data, it can be inferred that macrophages may contribute to the cellular mechanisms underlying CXCL8 overproduction during IVDD.

3.4. CXCL8/CXCR2 signaling participates in oxidative stress modulation and promotes ROS production

We proceeded to investigate the mechanisms by which CXCL8/CXCR2 mediates the inflammatory response in IVDD. Notably, we assessed the expression of genes related to CXCL8 using the Gene Set Enrichment Analysis (GSEA) tool. Our findings revealed a significant enrichment in reactive oxygen species (ROS) production and apoptosis. These results suggest a potential regulatory role of CXCL8 in the modulation of ROS and apoptosis process (Fig. 6a–b). We found that H2O2 and malondialdehyde (MDA) level were significantly increased in NP tissues from IVDD group vs vehicle group, whereas SB225002 treated group showed significantly reduced H2O2 and MDA level (Fig. 6c–d). In contrast, the levels of antioxidant enzymes superoxide dismutase (SOD) and glutathione peroxidase (GSH-Px) exhibited a substantial decrease in the NP tissues of IVDD group. However, rats treated with SB225002

demonstrated significantly enhanced levels of these enzymes when compared to the IVDD group, as depicted in Fig. 6e and f. TUNEL staining analysis revealed notable disparities in apoptosis between the IVDD group and the control groups. The group treated with SB225002 exhibited a substantial decrease in apoptosis levels within the NP tissue (Fig. 6g–h). Subsequently, we examined the impact of exogenously administered rCXCL8 on oxidative stress in the NP tissues of IVDD model. TUNEL analysis indicated an increase in the rate of apoptosis under rCXCL8 treatment, which was subsequently reduced in the IVDD + rCXCL8+SB225002 group (Fig. 6i–j). The injection of rCXCL8 in the IVDD group resulted in a further decrease in the activities of antioxidant enzymes SOD and GSH-Px, as well as an increase in H2O2 and MDA levels in NP tissues. Additionally, the elevated levels of H2O2 and MDA induced by rCXCL8 were reversed when co-administered with SB225002 (Fig. 6k-n). These findings collectively demonstrate that the CXCL8/CXCR2 pathway promotes apoptosis and the production of ROS in IVDD.

3.5. CXCL8 promotes NPCs apoptosis and the overproduction of ROS in vitro

Previously, CXCL8 was described to promote apoptosis and ROS overproduction in vivo. To study the effect of CXCL8 on apoptosis in vitro, we used the CXCR2 inhibitor SB225002 to halt the apoptosis process. Again, the levels of CXCR2 and MMP13 increased in the presence of CXCL8 but decreased in the presence of SB225002, COL2A1 showed an opposite trend (Fig. 7a–d). The apoptosis levels of NP cells exhibited a comparable trend to the WB outcome when examined through flow cytometry and IF staining. The flow cytometry assay revealed significantly higher apoptosis rates of NP cells in the CXCL8 and CXCL8+DMSO groups compared to the control group. However, this effect was rapidly reversed in the CXCL8+SB225002 group (Fig. 7e–f). IF demonstrated the co-localization of cleaved-caspase3 positive cells (green) and CXCR2-positive cells (red) in the NPCs following CXCL8 stimulation. The densitometry analysis graph demonstrates a decrease in the expression of CXCR2 and cleaved caspase-3 following the administration of SB225002 (Fig 7g and i-j). Our investigation focused on the intracellular ROS levels in NPCs upon stimulation with CXCL8. To mitigate CXCR2 activation, SB225002 was employed. Upon CXCL8 stimulation, there was a substantial increase in intracellular ROS content, which subsequently decreased rapidly upon the injection of SB225002 (Fig. 7h and k).

3.6. CXCL8/CXCR2 regulate NPCs apoptosis and ROS via the NF-κB signalling pathway

The involvement of the NF-κB signaling pathway in apoptosis and ROS production in NPCs has been supported by relevant literature and previous bioinformatic analyses [25,26]. In order to validate the participation of the NF-κB signaling pathway in this regulatory process, the phosphorylation of p65 (p-p65) and phosphorylation of IKBa (p-IKBa), both of which are metabolites associated with NF-κB activation, were assessed using WB. The results of the WB analysis demonstrated that the expression of p-p65 and p-IKBa was upregulated by CXCL8, but significantly reduced after treatment with SB225002 (Fig. 8a–c). IF analyses revealed an augmentation in nuclear staining of
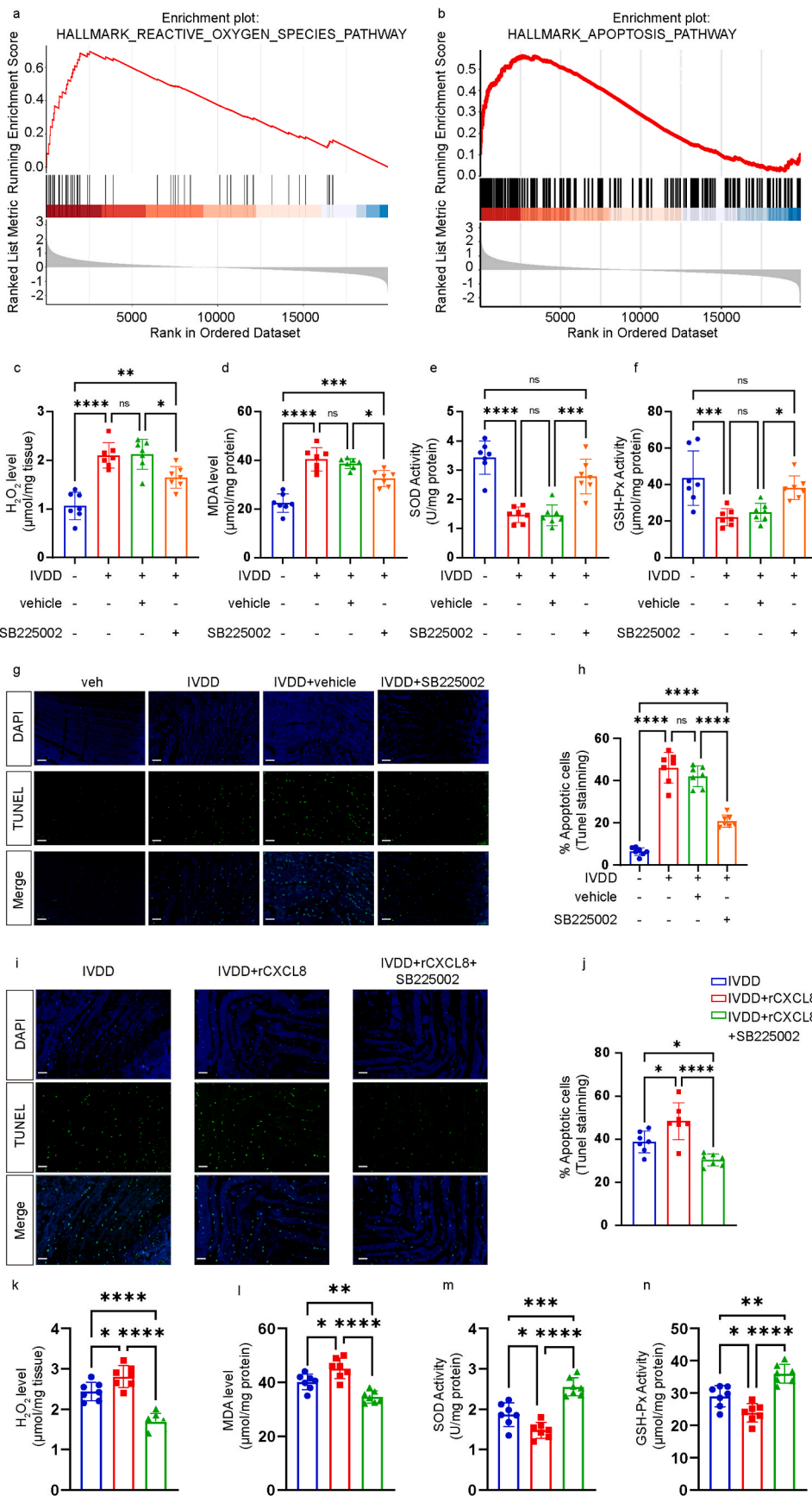
(caption on next page)

Fig. 6. CXCL8/CXCR2 signaling participates in oxidative stress modulation and promotes ROS production
(a-b) Gene Set Enrichment Analysis (GSEA) showed significant enriched in reactive oxygen species (ROS) production and apoptosis. (c–f) Summarized data showed H2O2 content (c), MDA content (d), SOD activity (e) and GSH-Px activity (f) in IVDs (N = 7 biological samples for each group). (g–j) Representative images of TUNEL assay (g and i) and quantification of apoptotic cells (h and j) by fluorescent TUNEL assay (N = 7 IVDs for each group). (k–n) Summarized data showed H2O2 content (k), MDA content (l), SOD activity (m) and GSH-Px activity (n) in IVDs after rescue experiment (N = 7 biological samples for each group). Data are represented mean ± s.e.m and were analysed using one-way ANOVA followed by Tukey's multiple-comparison test. *p < 0.05, **p < 0.01, ***p < 0.0001, ****p < 0.00001were considered significant difference, ns: non-significance.

p65 in the cells following CXCL8 stimulation, which was subsequently diminished after treatment with SB225002 (Fig. 8d–f). To inhibit activation of the NF-κB pathway, PDTC (100 μM) was employed. As depicted in Fig. 8g–j, PDTC effectively obstructed NF-κB signaling by reducing p-p65 expression. Consequently, MMP13 expression exhibited a declining pattern, while COL2A1 expression exhibited a significantly higher level. Subsequent assessment of apoptosis through flow cytometry assay yielded analogous findings, with lower rates of apoptosis observed in the PDTC-treated groups compared to the CXCL8 group (Fig. 8k). The content of ROS in NPCs was detected using a DCFH-DA probe. ROS contents were markedly attenuated by PDTC treatment, while no significant differences in the changes of ROS contents in the CXCL8+DMSO and CXCL8 groups were observed. This study demonstrated that the activation of CXCL8/CXCR2 results in heightened ROS production via the NF-κB signaling pathway, leading to increased expression of apoptotic proteins, degradation of the extracellular matrix, and ultimately, NPCs apoptosis.

4. Discussion

Cytokines play a crucial role in regulating IVDD [27]. As degeneration progresses, heightened levels of inflammatory cytokines expedite the IVDD process by intensifying the degradation of aggrecan and collagen, as well as promoting phenotypic changes in disc cells [7]. Additionally, inflammatory cytokines can induce the apoptosis of disc cells and ECM, thereby contributing to IVDD [28].

In this study, we first screened the potential inflammatory cytokines or chemokines in GSE27494/GSE41883 datasets. It was observed that CXCL8 emerged as one of the prominently up-regulated cytokines in IVDD. Subsequently in the study, it was observed that elevated levels of CXCL8 exhibited a positive correlation with degeneration of the disc, as determined by the degeneration grade. Furthermore, our research confirms the upregulation of CXCL8 and its receptor in highly degenerative human NP tissue. Similar to our findings, previous studies have also shown that mRNA for CXCL8 increased in the spinal cord and DRG in a rat model of lumbar disc herniation [29]. The degeneration of lumbar paravertebral muscles is a common occurrence in patients with IVDD, particularly in those with multifidus degeneration [30]. Our study also revealed significant variations in CXCL8 concentrations related to degeneration of the PM and LMM muscles. Finally, we found that CXCL8 concentrations were positively associated with the clinical severity of IVDD, as determined by the ODI index and VAS score. Our findings verified the results of previous studies, indicating the clinical importance of CXCL8 in degenerative disc disease. We hypothesized that CXCL8 functioned as a molecular marker and could potentially be employed in the clinical management of patients with IVDD.

Apart from regulating neutrophil recruitment and activation, in specific conditions, CXCL8 is described to regulate angiogenesis by stimulating migration and proliferation of CXCR2-expressing neovascularizing endothelial cells, forming new blood vessels [11,31]. CXCL8 has the potential to stimulate the activation of microglia, consequently impacting hyperalgesia. Furthermore, the observed delayed increase of CXCL8 expression in the spinal cord and DRG implies its potential significance in the perpetuation of chronic radicular neuropathic pain in the lumbar disc herniation model [29]. However, the precise mechanism by which CXCL8 interacts with the CXCR2 receptor to regulate intervertebral disc degeneration remains uncertain.

Subsequent neutralizing CXCL8 or inhibiting its receptor CXCR2 by

SB225002 demonstrated a significant reduction in the degree of IVDD. The interaction between CXCL8 and CXCR2 trigered the activation of the NF-κB pathway, leading to elevated levels of ROS in NPCs, which further induced apoptosis and degradation of the extracellular matrix in downstream NP cells. These findings collectively indicate a significant involvement of CXCL8/CXCR2 in IVDD. CXCL8 is primarily synthesized by various immune cells, including macrophages, T-lymphocytes, neutrophils, and other cell types, in response to an antigenic stimulus [11, 32]. During the initial stages of disc degeneration, macrophages are the predominant cell population that accumulates at the interface between NP and AF, in response to a low-grade inflammatory process [10,33]. Our in vitro experiments demonstrated that both the RAW264.7 macrophage cell line and cultured mouse peritoneal macrophages respond to LPS by producing CXCL8. The depletion of macrophages in vivo using clodronate resulted in a significant reduction in the upregulation of CXCL8 protein in NP tissues and further mitigated the degradation of the extracellular matrix in IVDD. This finding verified previous literature and provides the most direct evidence supporting the notion that macrophages produce CXCL8 in response to IVDD [21,22,34]. Consequently, our results suggest that macrophages may be one of the cellular sources responsible for the excessive production of CXCL8 during IVDD. However, it is important to consider the involvement of other tissues or cell types, such as annulus fibrosus cells and endplate chondrocytes, in the production of CXCL8 under inflammatory conditions. We do not know whether it has an indirect or direct influence on IVDD. We think CXCL8 might affect NP in both direct and indirect ways. On the one hand, CXCL8 might be distributed in the intervertebral disc and directly inhibit the apoptosis of NPCs. On the other hand, a variety of cytokines, chemokines, and other substances are secreted by tissues in the body to communicate with one another. Therefore, CXCL8 might exert its effects indirectly by influencing secretory phenotypes in other tissues not only in the intervertebral disc. Further experimentation is necessary to confirm this. However, it cannot be denied that CXCL8 remains a potential therapeutic target for IVDD, both directly and indirectly.

IVDD is often accompanied by oxidative stress, which leads to the generation of ROS in the IVDs [35,36]. H2O2 levels have been found to be significantly elevated in the NP tissues of a mouse IVDD model, resulting in apoptosis of NP cells and degradation of the extracellular matrix [37,38]. We conducted GSEA on DEGs associated with CXCL8 in our datasets to characterise the functions performed by CXCL8 as a synergistic gene. GSEA analysis showed that the expression of CXCL8 is associated with ROS and Apoptosis pathway. However, the precise mechanisms underlying the generation and modulation of oxidative stress in the context of IVDD remain incompletely elucidated. Our study demonstrated that the introduction of exogenous CXCL8 intensified oxidative stress, increased ROS production, and exacerbated NP apoptosis in IVDD. Conversely, administration of SB225002 resulted in a notable reduction in oxidative stress, ROS production, and NP apoptosis through a mechanism dependent on CXCR2. The findings of this study collectively indicate that CXCL8/CXCR2 plays a crucial role in regulating oxidative stress during IVDD.

The NF-κB signaling pathway plays an important role in mediating cellular responses to inflammation [39]. The inflammatory response and the activation of the NF-κB signaling pathway are involved in the progression of IVDD [40]. Previous studies showed that the activated NF-κB signaling pathway can promote the expression of inflammatory cytokines, increase the degradation of the ECM, and further deteriorate the
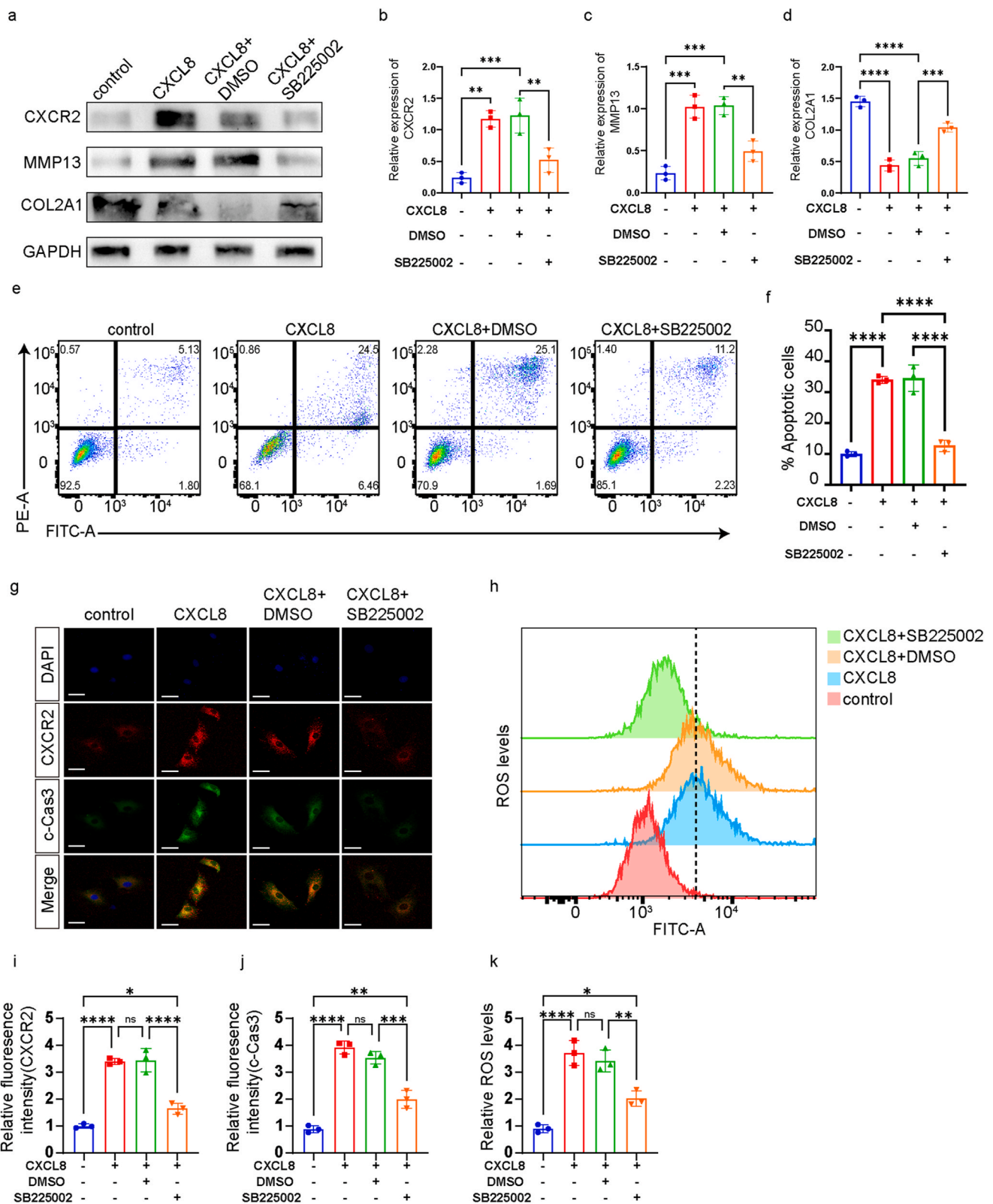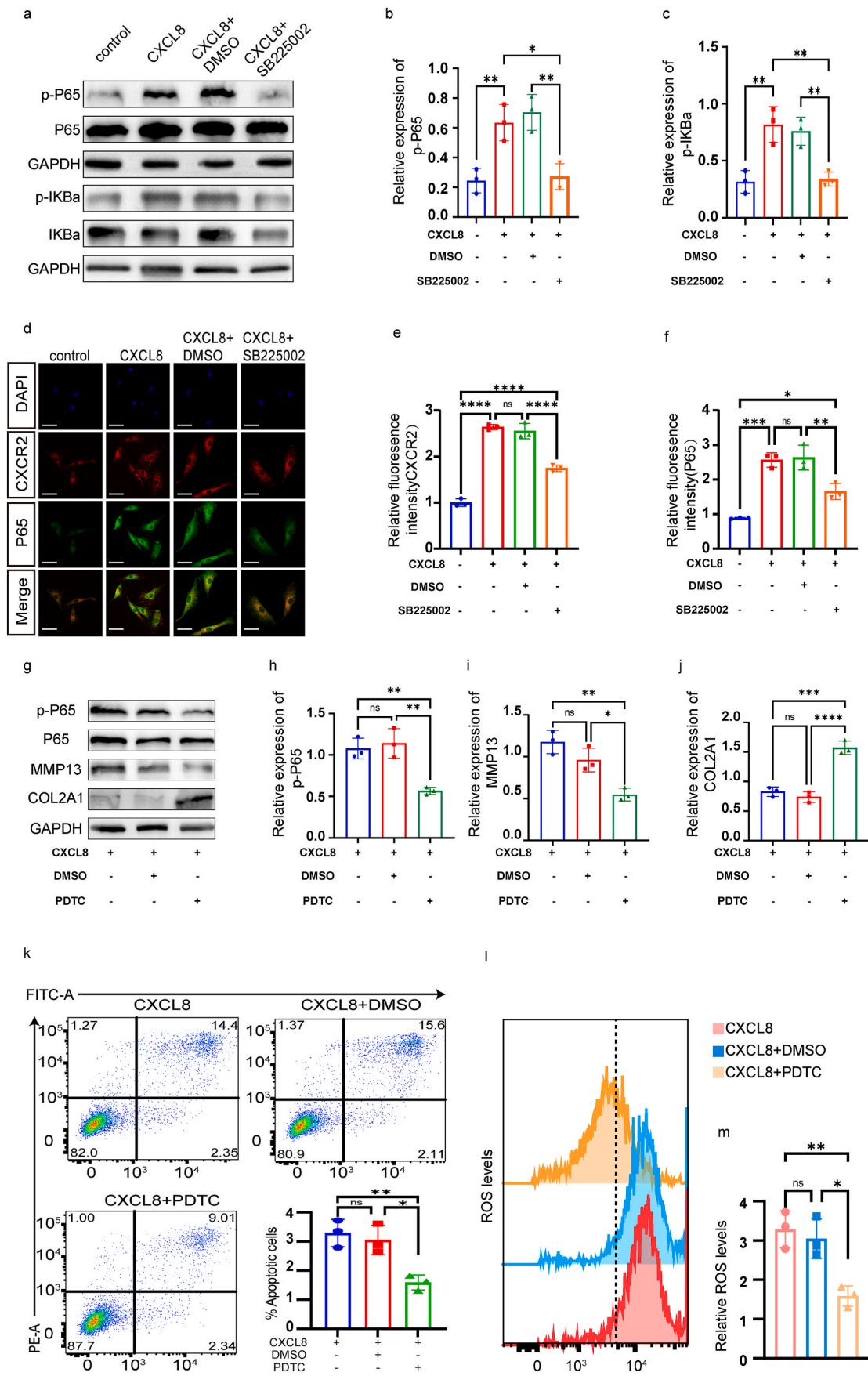
Fig. 7. CXCL8 promotes NPCs apoptosis and the overproduction of ROS in vitro

(a-d) Western blot analysis and quantification for CXCR2/MMP13/COL2A1 (N = 3 biological samples for each group). (e–f) Quantification of NP cell apoptosis by flow cytometry (N = 3 for each group). (g and i-j) IF assays showed the co-localization images of CXCR2 (red) and cleaved caspase-3 (green). Scale bar = 50 μm. Co-localization analysis (i and j) by evaluating relative fluorescence intensity. (h) Intracellular ROS levels detected by flow cytometry. (k) Quantification of ROS level (N = 3 for each group). Data are represented mean ± s.e.m and were analysed using one-way ANOVA followed by Tukey's multiple-comparison test. *$p < 0.05$, **$p < 0.01$, ***$p < 0.0001$, ****$p < 0.00001$ were considered significant difference, ns: non-significance. (For interpretation of the references to color in this figure legend, the reader is referred to the Web version of this article.)

(caption on next page)

Fig. 8. CXCL8/CXCR2 regulate NPCs apoptosis and ROS via NF-κB signalling pathway
(a-c) Western blot detection (a) and grey value analysis (b–c) of p-p65 and p-IKBa level (N = 3 biological samples for each group). (d–f) IF assays showed the co-localisation of CXCR2 (red) and p65 (green), Scale bar = 50 µm. Co-localization analysis (e and f) by evaluating relative fluorescence intensity (N = 3 IVDs for each group). (g–j) Western blot analysis and quantification for p-p65/MMP13/COL2A1 (N = 3 biological samples for each group). (k) Quantification of NP cell apoptosis after PDTC administration by flow cytometry (N = 3 for each group). (l) Intracellular ROS levels detected by flow cytometry. (m) Quantification of ROS level (N = 3 for each group). Data are represented mean ± s.e.m and were analysed using one-way ANOVA followed by Tukey's multiple-comparison test. *p < 0.05, **p < 0.01, ***p < 0.0001, ****p < 0.00001 were considered significant difference, ns: non-significance. (For interpretation of the references to color in this figure legend, the reader is referred to the Web version of this article.)

progression of IVDD [25,41]. Therefore, inhibition of the NF-κB signaling pathway can retard the process of IVDD.

In our study, it was observed that CXCL8 effectively activated the NF-κB signaling pathway, leading to an increase in the level of p-P65 in NPCs. However, this heightened activation was successfully suppressed through the administration of SB225002. These findings suggest that SB225002 has the potential to serve as a therapeutic approach for mitigating the effects of IVDD by inhibiting CXCL8-induced activation of the NF-κB signaling pathway. Additionally, it is worth noting that CXCL8 may also contribute to the release of MMP-13, thereby exerting a positive influence on the degradation of ECM and ROS overproduction, thus causing apoptosis of NP cells.

5. Conclusions

Specifically, our research has revealed a previously unrecognized function of CXCL8/CXCR2 in mediating apoptosis of NP cells and degradation of the extracellular matrix in IVDD, achieved by promoting the production of ROS through the activation of NF-κB. Consequently, our study proposes that targeting the CXCL8/CXCR2 signaling pathway could serve as a promising therapeutic strategy for alleviating intervertebral disc degeneration.

Author contribution statement

Pengfei XueLong LvLei LiuYuzhu XuChonggang ZhouYuntao Wang

Funding

Data availability

The data that support the findings in this study are available from the corresponding author upon reasonable request.

Declaration of Competing interest

All the authors listed assure that the data in the manuscript is original and the manuscript is not under consideration elsewhere. None of the manuscript contents have been previously published. All authors have made significant contributions of this work, and have read and approved all versions of the manuscript, its content, and its submission to the journal.

The authors have no conflict of interests.

Appendix A. Supplementary data

Supplementary data to this article can be found online at https://doi.org/10.1016/j.jot.2024.08.022.

References

[1] Xiang H, Zhao W, Jiang K, He J, Chen L, Cui W, et al. Progress in regulating inflammatory biomaterials for intervertebral disc regeneration. Bioact Mater Mar 2024;33:506–31. https://doi.org/10.1016/j.bioactmat.2023.11.021.

[2] Gao Y, Chen X, Zheng G, Lin M, Zhou H, Zhang X. Current status and development direction of immunomodulatory therapy for intervertebral disk degeneration. Front Med 2023;10:1289642. https://doi.org/10.3389/fmed.2023.1289642.

[3] Luo Z, Wei Z, Zhang G, Chen H, Li L, Kang X. Achilles' heel-the significance of maintaining microenvironmental homeostasis in the nucleus pulposus for intervertebral discs. Int J Mol Sci Nov 22 2023;24(23). https://doi.org/10.3390/ijms242316592.

[4] Sun Y, Lyu M, Lu Q, Cheung K, Leung V. Current perspectives on nucleus pulposus fibrosis in disc degeneration and repair. Int J Mol Sci Jun 14 2022;23(12). https://doi.org/10.3390/ijms23126612.

[5] Liu Y, Dou Y, Sun X, Yang Q. Mechanisms and therapeutic strategies for senescence-associated secretory phenotype in the intervertebral disc degeneration microenvironment. Journal of orthopaedic translation Mar 2024;45:56–65. https://doi.org/10.1016/j.jot.2024.02.003.

[6] Karchevskaya AE, Poluektov YM, Korolishin VA. Understanding intervertebral disc degeneration: background factors and the role of initial injury. Biomedicines Oct 6 2023;11(10). https://doi.org/10.3390/biomedicines11102714.

[7] Lu R, Xu H, Deng X, Wang Y, He Z, Xu S, et al. Physalin A alleviates intervertebral disc degeneration via anti-inflammatory and anti-fibrotic effects. Journal of orthopaedic translation Mar 2023;39:74–87. https://doi.org/10.1016/j.jot.2023.01.001.

[8] Xu H, Li J, Fei Q, Jiang L. Contribution of immune cells to intervertebral disc degeneration and the potential of immunotherapy. Connect Tissue Res Sep 2023;64 (5):413–27. https://doi.org/10.1080/03008207.2023.2212051.

[9] Feng P, Che Y, Gao C, Zhu L, Gao J, Vo NV. Immune exposure: how macrophages interact with the nucleus pulposus. Front Immunol 2023;14:1155746. https://doi.org/10.3389/fimmu.2023.1155746.

[10] Koroth J, Buko EO, Abbott R, Johnson CP, Ogle BM, Stone LS, et al. Macrophages and intervertebral disc degeneration. Int J Mol Sci Jan 10 2023;24(2). https://doi.org/10.3390/ijms24021367.

[11] Cambier S, Gouwy M, Proost P. The chemokines CXCL8 and CXCL12: molecular and functional properties, role in disease and efforts towards pharmacological intervention. Cell Mol Immunol Mar 2023;20(3):217–51. https://doi.org/10.1038/s41423-023-00974-6.

[12] Dhayni K, Zibara K, Issa H, Kamel S, Bennis Y. Targeting CXCR1 and CXCR2 receptors in cardiovascular diseases. Pharmacol Therapeut Sep 2022;237:108257. https://doi.org/10.1016/j.pharmthera.2022.108257.

[13] Dudli S, Haschtmann D, Ferguson SJ. Fracture of the vertebral endplates, but not equienergetic impact load, promotes disc degeneration in vitro. J Orthop Res : official publication of the Orthopaedic Research Society May 2012;30(5):809–16. https://doi.org/10.1002/jor.21573.

[14] Risbud MV, Shapiro IM. Role of cytokines in intervertebral disc degeneration: pain and disc content. Nat Rev Rheumatol Jan 2014;10(1):44–56. https://doi.org/10.1038/nrrheum.2013.160.

[15] Issy AC, Castania V, Castania M, Salmon CE, Nogueira-Barbosa MH, Bel ED, et al. Experimental model of intervertebral disc degeneration by needle puncture in Wistar rats. Brazilian journal of medical and biological research = Revista brasileira de pesquisas medicas e biologicas Mar 2013;46(3):235–44. https://doi.org/10.1590/1414-431x20122429.

[16] Meftahi GH, Bahari Z, Zarei Mahmoudabadi A, Iman M, Jangravi Z. Applications of western blot technique: from bench to bedside. Biochem Mol Biol Educ : a bimonthly publication of the International Union of Biochemistry and Molecular Biology Jul 2021;49(4):509–17. https://doi.org/10.1002/bmb.21516.

[17] Han B, Zhu K, Li FC, Xiao YX, Feng J, Shi ZL, et al. A simple disc degeneration model induced by percutaneous needle puncture in the rat tail. Spine Aug 15 2008;33(18):1925–34. https://doi.org/10.1097/BRS.0b013e31817c64a9.

[18] Wang Y, Che M, Xin J, Zheng Z, Li J, Zhang S. The role of IL-1β and TNF-α in intervertebral disc degeneration. Biomedicine & pharmacotherapy = Biomedecine & pharmacotherapie Nov 2020;131:110660. https://doi.org/10.1016/j.biopha.2020.110660.

[19] Tan Y, Wang X, Zhang Y, Dai Z, Li J, Dong C, et al. FOXO3-Activated circFGFBP1 inhibits extracellular matrix degradation and nucleus pulposus cell death via miR-9-5p/BMP2 Axis in intervertebral disc degeneration in vivo and in vitro. Pharmaceuticals Mar 22 2023;16(3). https://doi.org/10.3390/ph16030473.

[20] Pfirrmann CW, Metzdorf A, Zanetti M, Hodler J, Boos N. Magnetic resonance classification of lumbar intervertebral disc degeneration. Spine Sep 1 2001;26(17):1873–8. https://doi.org/10.1097/00007632-200109010-00011.

[21] Ye F, Lyu FJ, Wang H, Zheng Z. The involvement of immune system in intervertebral disc herniation and degeneration. JOR spine Mar 2022;5(1):e1196. https://doi.org/10.1002/jsp2.1196.

[22] Takada T, Nishida K, Maeno K, Kakutani K, Yurube T, Doita M, et al. Intervertebral disc and macrophage interaction induces mechanical hyperalgesia and cytokine production in a herniated disc model in rats. Arthritis Rheum Aug 2012;64(8):2601–10. https://doi.org/10.1002/art.34456.

[23] James G, Chen X, Diwan A, Hodges PW. Fat infiltration in the multifidus muscle is related to inflammatory cytokine expression in the muscle and epidural adipose tissue in individuals undergoing surgery for intervertebral disc herniation. Eur Spine J Apr 2021;30(4):837–45. https://doi.org/10.1007/s00586-020-06514-4. official publication of the European Spine Society, the European Spinal Deformity Society, and the European Section of the Cervical Spine Research Society.

[24] Goutallier D, Postel JM, Bernageau J, Lavau L, Voisin MC. Fatty muscle degeneration in cuff ruptures. Pre- and postoperative evaluation by CT scan. Clin Orthop Relat Res Jul 1994;304:78–83.

[25] Zhang GZ, Liu MQ, Chen HW, Wu ZL, Gao YC, Ma ZJ, et al. NF-κB signalling pathways in nucleus pulposus cell function and intervertebral disc degeneration. Cell Prolif Jul 2021;54(7):e13057. https://doi.org/10.1111/cpr.13057.

[26] Li S, Pan X, Wu Y, Tu Y, Hong W, Ren J, et al. IL-37 alleviates intervertebral disc degeneration via the IL-1R8/NF-κB pathway. Osteoarthritis Cartilage May 2023;31 (5):588–99. https://doi.org/10.1016/j.joca.2023.01.006.

[27] Chen X, Wang Z, Deng R, Yan H, Liu X, Kang R. Intervertebral disc degeneration and inflammatory microenvironment: expression, pathology, and therapeutic strategies. Inflamm Res. Sep 2023;72(9):1811–28. https://doi.org/10.1007/s00011-023-01784-2.

[28] Shnayder NA, Ashhotov AV, Trefilova VV, Nurgaliev ZA, Novitsky MA, Vaiman EE, et al. Cytokine imbalance as a biomarker of intervertebral disk degeneration. Int J Mol Sci Jan 25 2023;24(3). https://doi.org/10.3390/ijms24032360.

[29] Kim SJ, Park SM, Cho YW, Jung YJ, Lee DG, Jang SH, et al. Changes in expression of mRNA for interleukin-8 and effects of interleukin-8 receptor inhibitor in the spinal dorsal horn in a rat model of lumbar disc herniation. Spine Dec 1 2011;36 (25):2139–46. https://doi.org/10.1097/BRS.0b013e31821945a3.

[30] Kalichman L, Carmeli E, Been E. The association between imaging parameters of the paraspinal muscles, spinal degeneration, and low back pain. BioMed Res Int 2017;2017:2562957. https://doi.org/10.1155/2017/2562957.

[31] Sitaru S, Budke A, Bertini R, Sperandio M. Therapeutic inhibition of CXCR1/2: where do we stand? Internal and emergency medicine Sep 2023;18(6):1647–64. https://doi.org/10.1007/s11739-023-03309-5.

[32] Xiong X, Liao X, Qiu S, Xu H, Zhang S, Wang S, et al. CXCL8 in tumor biology and its implications for clinical translation. Front Mol Biosci 2022;9:723846. https://doi.org/10.3389/fmolb.2022.723846.

[33] Wu XT, Wang YX, Feng XM, Feng M, Sun HH. Update on the roles of macrophages in the degeneration and repair process of intervertebral discs. Joint Bone Spine May 2023;90(3):105514. https://doi.org/10.1016/j.jbspin.2022.105514.

[34] Russo RC, Garcia CC, Teixeira MM, Amaral FA. The CXCL8/IL-8 chemokine family and its receptors in inflammatory diseases. Expet Rev Clin Immunol May 2014;10 (5):593–619. https://doi.org/10.1586/1744666x.2014.894886.

[35] Yao D, Chen E, Li Y, Wang K, Liao Z, Li M, et al. The role of endoplasmic reticulum stress, mitochondrial dysfunction and their crosstalk in intervertebral disc degeneration. Cell Signal Feb 2024;114:110986. https://doi.org/10.1016/j.cellsig.2023.110986.

[36] Wang Y, Cheng H, Wang T, Zhang K, Zhang Y, Kang X. Oxidative stress in intervertebral disc degeneration: molecular mechanisms, pathogenesis and treatment. Cell Prolif Sep 2023;56(9):e13448. https://doi.org/10.1111/cpr.13448.

[37] Zhang YY, Hu ZL, Qi YH, Li HY, Chang X, Gao XX, et al. Pretreatment of nucleus pulposus mesenchymal stem cells with appropriate concentration of H(2)O(2) enhances their ability to treat intervertebral disc degeneration. Stem Cell Res Ther Jul 26 2022;13(1):340. https://doi.org/10.1186/s13287-022-03031-7.

[38] Liu L, Zhang Y, Fu J, Ai X, Long D, Leng X, et al. Gli1 depletion induces oxidative stress and apoptosis of nucleus pulposus cells via Fos in intervertebral disc degeneration. Journal of orthopaedic translation May 2023;40:116–31. https://doi.org/10.1016/j.jot.2023.05.008.

[39] Baker RG, Hayden MS, Ghosh S. NF-κB, inflammation, and metabolic disease. Cell Metabol Jan 5 2011;13(1):11–22. https://doi.org/10.1016/j.cmet.2010.12.008.

[40] Wang P, Yang C, Lu J, Ren Y, Goltzman D, Miao D. Sirt1 protects against intervertebral disc degeneration induced by 1,25-dihydroxyvitamin D insufficiency in mice by inhibiting the NF-κB inflammatory pathway. Journal of orthopaedic translation May 2023;40:13–26. https://doi.org/10.1016/j.jot.2023.04.003.

[41] Sun Z, Yin Z, Liu C, Tian J. The changes in the expression of NF-KB in a degenerative human intervertebral disc model. Cell Biochem Biophys May 2015;72 (1):115–22. https://doi.org/10.1007/s12013-014-0417-3.